ACS APPLIED MATERIALS & INTERFACES

www.acsami.org

Research Article

Wafer-Scale Full-Coverage Self-Limiting Assembly of Particles on Flexible Substrates

Liang Zhao, Bchara Sidnawi, Jichao Fan, Ruiyang Chen, Thomas Scully, Scott Dietrich, Weilu Gao, Qianhong Wu, and Bo Li*

Cite This: https://doi.org/10.1021/acsami.2c14149

Read Online

ACCESS | Metrics & More | Article Recommendations | Supporting Information

ABSTRACT: Self-limiting assembly of particles represents the state-of-the-art controllability in nanomanufacturing processes where the assembly stops at a designated stage, providing a desirable platform for applications requiring delicate thickness control such as optics, electronics, and catalytic systems. Most successes in self-limiting assembly are limited to self-assembled monolayers (SAMs) of small molecules on inorganic, chemically homogeneous rigid substrates (e.g., Au and SiO_2) through surface−interaction mechanisms. Similar mechanisms, however, cannot achieve a uniform assembly of particles on flexible polymer substrates. The complex configurations and conformations of polymer chains create a surface with nonuniform distributions of chemical groups and phases. In addition, most assembly mechanisms require good solvent wettability, where many desirable but hard-to-wet particles and polymer substrates are excluded. Here, we demonstrate a collision-based self-limiting assembly (CSA) to achieve wafer-scale, full-coverage, close-packed monolayers of hydrophobic particles on hydrophobic polymer substrates in aqueous solutions. The kinetic assembly and self-limiting processes are facilitated and controlled by the combined acoustic and shear fields. We envision many applications in functional coatings and showcase their feasibility in structural coloration. Importantly, such functional coatings can be repaired using CSA, and both particles and polymer substrate can be recycled.

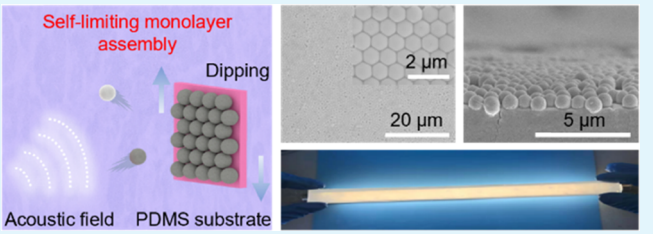

KEYWORDS: *self-limiting assembly, monolayer, structural coloration, recyclable, repairable*

INTRODUCTION

Self-assembled monolayers (SAMs) of molecules and particles show significant potential in applications such as molecular junctions,[1−3] ultrathin dielectrics,[4,5] chemical and biosensors,[6,7] adjustable wetting/protection coatings,[8−10] and medicines.[11] SAM was originally developed for molecules based on the self-limiting chemisorption process, which involves an accurate chemical design to create the buffer layer as a bridge between the substrate and SAM molecules.[12,13] When nano- or micro-particles are decorated with the SAM molecules, the self-limiting assembly of particles on target substrates can be achieved.[14] To achieve high-quality assembly with densely packed structures, a molecular-level chemically uniform surface of the substrate is required.[15] However, for polymers with complex configurations and conformations, it is extremely difficult to control the distribution of chemical groups or phases (e.g., amorphous and crystalline regions for semicrystalline polymers).[16] To improve the chemical uniformity, mechanical stretching has been utilized.[17] Unfortunately, self-limiting, high-density, and low-defect particle assembly on flexible polymer substrates is yet to be achieved for both molecules[17,18] and molecule-decorated particles.[16,19] Although chemical treatments can be used to modify the surface properties of particles and polymer substrates, a uniform chemical treatment for polymers remains a significant challenge.

If a self-limiting mechanism does not exist in a solution-based assembly process, the monolayer assembly of high-density particles must be achieved through the delicate control of the assembly parameters. The most successful strategy is to control the thickness of the ultrathin solution wetting layer on the substrate and the particle concentration, such that the amount of particles in the wetting layer is just enough to form a monolayer deposition after solvent evaporation. Following this strategy, researchers have realized monolayer particle assembly through the dip-coating process by controlling the withdrawing speed and tilting angle of the substrate,[20] the spin-coating process by controlling the spinning speed,[21,22] and the roll-to-roll process by controlling the rolling speed.[23] In addition, the densely packed monolayer structure can be realized through fast solvent evaporation, which significantly increases the capillary forces

Received: August 6, 2022
Accepted: September 21, 2022

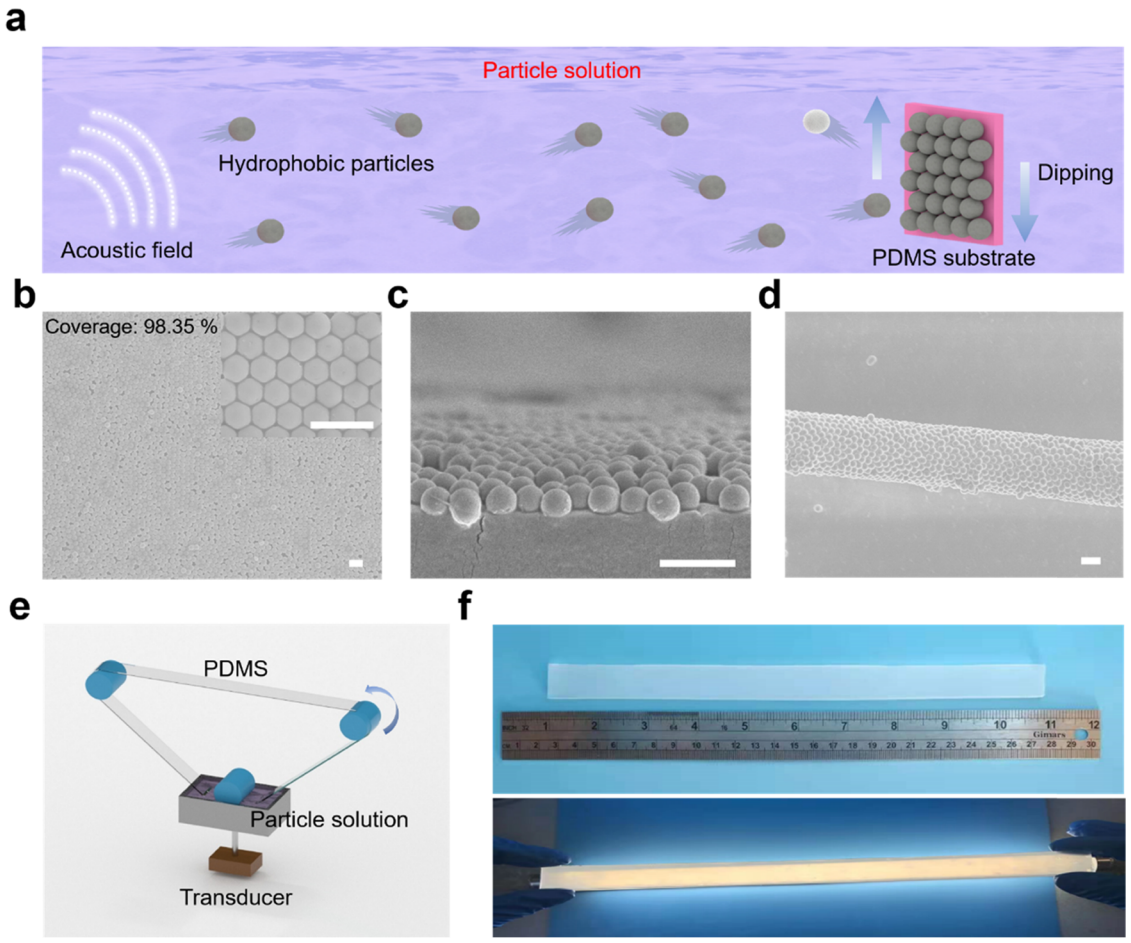

Figure 1. Monolayer assembly by CSA. (a) Schematic of the CSA process. (b) SEM image of a monolayer of SiO_2 particles (1007 ± 29 nm) on a PDMS (10:1) substrate. The inset is at high magnification and displays the local hexagonal structure of the particles. (c) The cross-sectional view of monolayer SiO_2 particles. (d) Monolayer SiO_2 particles assembled on a PDMS (10:1) fiber. All scale bars, 2 μm. (e) Schematic of the large-scale manufacturing of monolayer SiO_2 particles on the PDMS substrate. (f) Photo of the resulting large-area monolayer of SiO_2 particles on a PDMS substrate (top) and the produced orange color from a white light source (bottom).

among particles.[15,20] However, these dense monolayer particle structures are achieved at the high cost of controlling the manufacturing process and low productivity. Here, we develop a collision-based self-limiting assembly (CSA) method where the collision between monodispersed particles and a viscoelastic polymer substrate is facilitated by acoustic and flow fields to realize high-rate, close-packed monolayer assembly of nano-/microparticles. Importantly, the assembly terminates once the monolayer forms, and the monolayer film's quality is not sensitive to solution concentration and assembly time, thus paving the way for low-cost and high-quality manufacturing of monolayer particles on flexible substrates.

RESULTS AND DISCUSSION

The assembly process is outlined in Figure 1a. In contrast to the SAM created by the chemisorption of molecules with head groups interacting with the substrate,[24] CSA represents a new assembly mechanism based on physical interactions. The hydrophobic monodisperse silica (SiO_2) particles with a very narrow size distribution (three diameters: d = 487 ± 10, 761 ± 25, and 1007 ± 29 nm) are dispersed and agitated by the acoustic field (frequency = 40 kHz, power density = 0.3 W cm^{-2}) in a water solution to collide with a moving poly(dimethylsiloxane) (PDMS, Sylgard 184) substrate driven by a customized dipping system to provide cyclic dipping (Figure S1). The viscoelastic polymer substrate attenuates the particle's kinetic energy upon collision, after which hydrophobic particles tend to stay on the hydrophobic substrate to minimize their surface energy in the water solution. Once the first particle layer forms, it becomes a hard shell on the substrate and prevents further deposition, leading to a self-limiting monolayer assembly. Such a mechanism relies on hard-to-wet surface energy design, viscoelastic polymer substrate dissipating the kinetic energy of particles, acoustic-field-induced particle dispersion and energization, and the fluid shearing at the substrate's surface. The hydrophobicity of the particles enables them to adhere to the soft PDMS substrate due to the lower surface energy between their surface and the substrates. This is corroborated by our previous assembly work on a wide range of hydrophobic nanomaterials (e.g., graphene, h-BN, carbon black, and carbon nanotube) on hydrophobic polymer substrates (e.g., PDMS and thermoplastic polyurethane).[25,26] However, the self-limiting monolayer mechanism has yet to be established because of the complex influence from the large size distribution of unsorted nanoparticles and limited understanding of acoustic and shear fields in the assembly process. The functions of acoustic and shear fields will be discussed separately in the following section. Here, we use monodispersed SiO_2 particles to achieve uniform monolayer assembly. The as-received SiO_2 particles are hydrophilic. The characterization of particle sizes

https://doi.org/10.1021/acsami.2c14149
ACS Appl. Mater. Interfaces XXXX, XXX, XXX−XXX

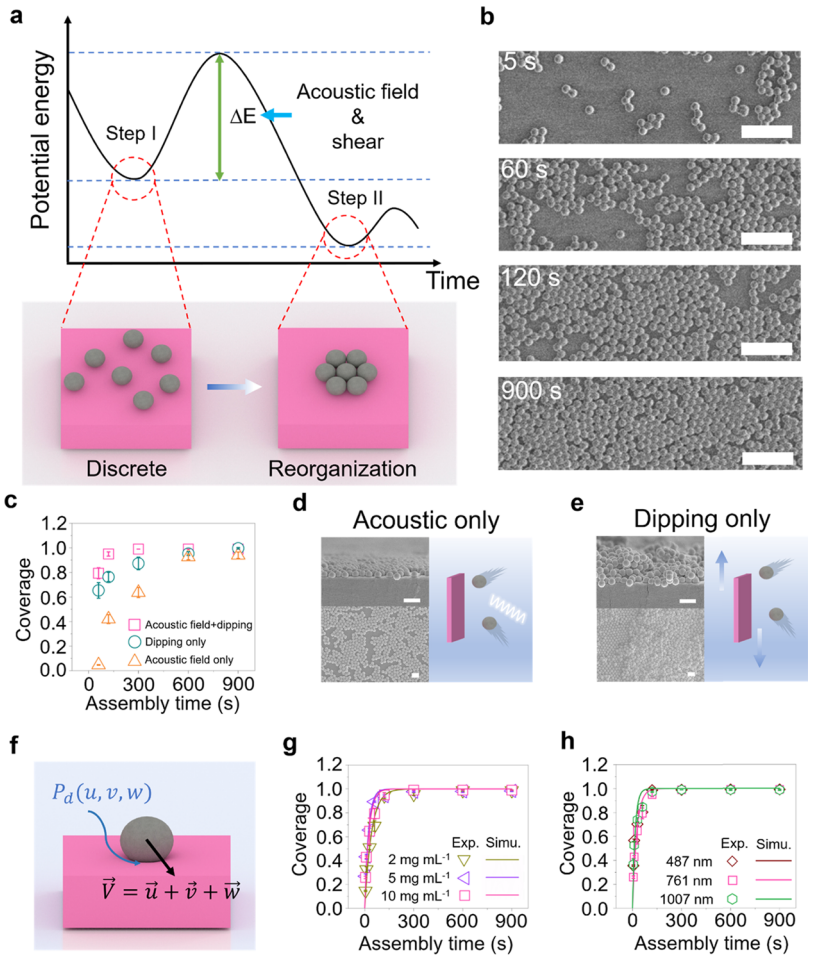

Figure 2. Self-limiting assembly monolayer mechanism from thermodynamic and kinetic perspectives. (a) Potential energy evolution with respect to assembly time and schematic of particle reorganization during the assembly process. ΔE represents the potential energy barrier. (b) SEM images of particle reorganization. Scale bars, 5 μm. (c) Coverage evolution using acoustic field + dipping, acoustic only, and dipping only. (d, e) Planar and cross-sectional SEM images of SiO_2 particles onto the PDMS substrate (761 nm, 10 mg mL^{-1}) after a 15 min assembly using different methods and their corresponding assembly schematics. (d) Acoustic only. (e) Dipping only. All scale bars in panels (d) and (e), 2 μm. (f) A diagram of the collision and adhesion process of a single particle on a polymer substrate. (g) Experiment and simulation of coverage evolution at different concentrations of SiO_2 (761 nm in diameter) and (h) same concentration (10 mg mL^{-1}) with different SiO_2 diameters.

by scanning electron microscope (SEM) and atomic force microscope (AFM) can be found in Figure S2. They are later modified with (3-aminopropyl) triethoxysilane (APTES) to create a hydrophobic surface (see surface chemistry and wettability characterization in Figures S3 and S4). Figure 1b,c demonstrates a close-packed monolayer of SiO_2 particles (d = 761 nm) on a flat PDMS substrate, and the coverage (δ) of the assembly can reach 98.35%. Note that a patch on which particles are closely packed is considered fully covered since no further material can fill the residual voids dictated by the particles' spherical geometry. The concentration (C_0) of particle suspension is 10 mg ml^{-1}, and the assembly time (t) is 900 s. Note that the pristine hydrophilic SiO_2 particles can achieve little assembly following identical procedures (Figure S5). The same principles can be extended to organic particles such as poly (methyl methacrylate) (PMMA) particles (d = 5 μm) (Figure S6a). Such a self-limiting mechanism is not sensitive to the geometry of the substrate. We have demonstrated the conformal coating of SiO_2 particles (d = 761 nm) on a PDMS microfiber (d = 6 μm) (Figure 1d) and PMMA particles (d = 5 μm) on microtrenched PDMS (Figure S6b). Importantly, CSA can be implemented within a roll-to-roll process to enable wafer-scale manufacturing, as shown in Figures 1e and S7, and Supplementary Video 1. The assembled monolayer of SiO_2 particles (d = 761 nm) shows a uniform orange color (Figure 1f) when illuminated with white light from the background, highlighting its potential for structural coloration.

Thermodynamically, the close-packed monolayer assembly takes place through two steps (Figure 2a): random adsorption (the local minimum in the energy diagram) and reorganization (the global minimum). However, for a SAM process, the transition from step I to step II takes hours to days.[15,17] In CSA, such a transition occurs on the order of minutes. It would be intuitively anticipated that the integration of acoustic and shear fields significantly facilitates overcoming the potential energy barrier (ΔE). Because both fields are applied throughout the assembly process, adsorption and reorganization occur simultaneously, as demonstrated in Figure 2b. At 5 s into the assembly, we observe randomly distributed particles with sporadic small aggregates. At 60 s, particles aggregate into bigger patches. At 120 s, a continuous monolayer with random voids is achieved. At 900 s, a close-packed monolayer is formed. Longer assembly times can further reorganize the network and reduce defects. To accurately track the assembly kinetics (coverage δ vs assembly

https://doi.org/10.1021/acsami.2c14149
ACS Appl. Mater. Interfaces XXXX, XXX, XXX−XXX

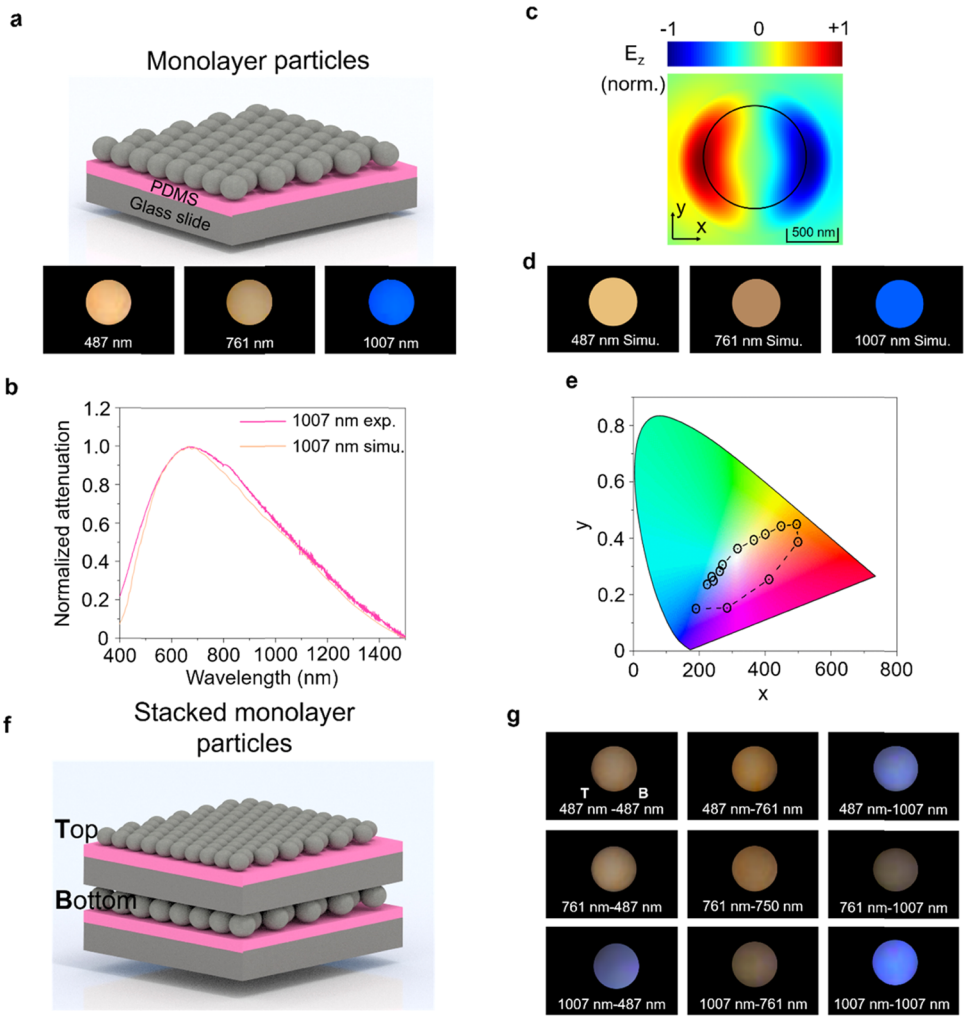

Figure 3. Structural coloration of monolayer SiO_2 assembled by CSA. (a) Schematic of the assembled monolayer SiO_2 on PDMS-coated glass slide and structural coloration with respect to various SiO_2 diameters. (b) Experimental and simulation scattering spectra of monolayer SiO_2 (1007 nm in diameter) particles. (c) The simulation electric field distribution of magnetic dipole (MD) mode at 0.66 μm. (d) Simulation color images based on measured sample parameters. (e) CIE1931 chromaticity diagram and simulation color space values obtained from scattering spectra of the SiO_2 nanosphere. (f) Schematic of stacked monolayer SiO_2 particles. (g) Structural coloration based on stacked monolayer SiO_2 particles and number pair indicates the stacking order where the left number indicates the diameter of the particle on the bottom layer and the right number indicates the diameter of the particle on the top layer. Note that here B and T represent the bottom layer and top layer with different or same particle sizes according to the stacking sequence, respectively.

time t), we fix three observation locations on the same substrate, and the SEM images taken from the three locations at the same assembly time are averaged to obtain the coverage (Figures S8 and S9).

To elucidate the functions of acoustic and shear fields, we fix the particle size and concentration ($d = 761 \pm 10$ nm and $C_0 = 10$ mg mL^{-1}) and compare the assembly kinetics for CSA (Figure 1b), assembly with acoustic field only (acoustic only), and assembly with shear field only (dipping only) (Figures 2c–e, S8, and S9c). The other assembly parameters are similar among the three while we simply turn off the dipping motor (acoustic only) or acoustic transducer (dipping only). The comparison suggests that CSA, combining both acoustic and shear fields, leads to the fastest assembly (Figure 2c). For morphology comparison at the same assembly time (t = 900 s), CSA leads to a close-packed assembly (Figure 1b), while acoustic-only process results in partial coverage (Figure 2d) and dipping-only process leads to multilayer structures (Figure 2e). The acoustic effect prevents particle aggregation in the solution and therefore keeps them from stacking up as clumps on the substrate (top image, Figure 2d). Coverage, however, is abated by the absence of the shear that would have been provided by cyclic dipping. The shear on the substrate's surface helps the particles penetrate the thinning water film separating from the substrate during their collision with it, therefore enhancing the coverage, as shown in Figure 2e. However, a monolayer can be hardly observed as self-assembly of aggregated nanoparticles in the solution may occur (top image, Figure 2e). Combining cyclic dipping with acoustic actuation not only leads to a monolayer covering the entire surface but also ensures a faster assembly than one that is driven by either an acoustic field or dipping only.

Figure 2f elaborates the mechanism of CSA on a polymer substrate. A particle heading toward the substrate at a velocity vector $\vec{V}$, consisting of a normal component, $\vec{w}$, and in-plane components, $\vec{u}$ and $\vec{v}$, will induce a deformation on the flexible surface upon collision. $g(u,v,w)$ describes the particles' velocity distribution prior to surface impact, while $P_d(u,v,w)$ describes the particle deposition probability. Another striking particle is

https://doi.org/10.1021/acsami.2c14149
ACS Appl. Mater. Interfaces XXXX, XXX, XXX−XXX

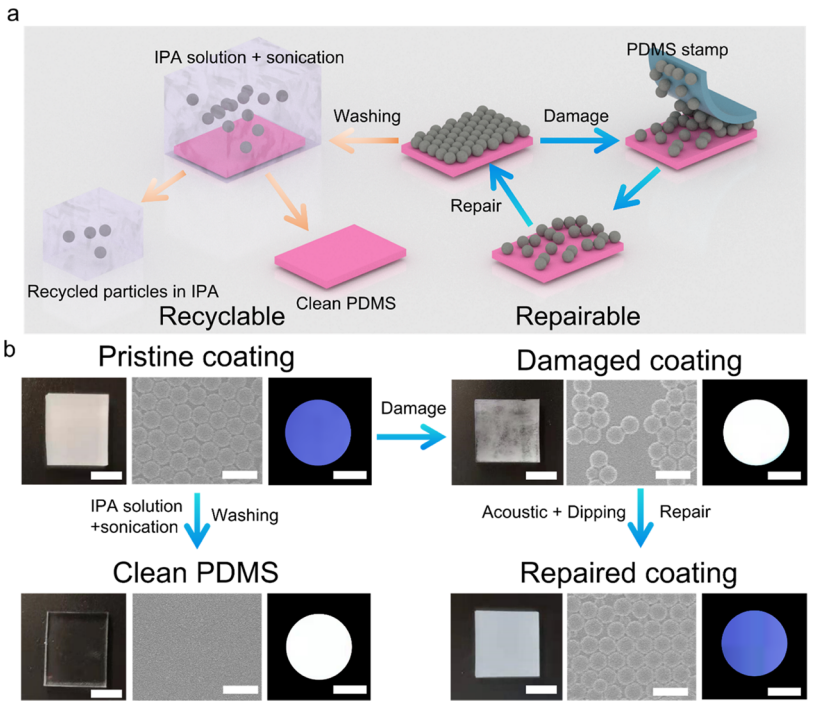

Figure 4. Repairability and recyclability of monolayer SiO_2 particle coatings on PDMS. (a) Schematic of the SiO_2 particles and PDMS recycling process using IPA solution washing with sonication, and repairing of the damaged SiO_2 monolayer structure. (b) Digital images (left), SEM images (middle), and structural coloration (right) of the monolayer SiO_2 on PDMS at different stages. Scale bars for digital images, SEM images, and structural coloration are 2 cm, 2 μm, and 5 mm, respectively.

much more likely to bounce off an already assembled monolayer due to both the hard collision and the acoustic field maintaining dispersion. The time evolution of the substrate's covered fraction,[27] $\delta(t) = 1 - e^{-\alpha C_0 a_p t}$, depends on the single particle's occupied area on the substrate, a_p, the particles' mass concentration C_0, and $\alpha = \frac{1}{m}\int_{\infty}^{-\infty}\int_{\infty}^{-\infty}\int_{\infty}^{0} wg(u, v, w)P_d(u, v, w)\mathrm{d}w\ \mathrm{d}u\ \mathrm{d}v$, where m is the single particle mass. Figure 2g shows representative fitting results of the equation for $\delta(t)$ for a particle size of 761 nm at different concentrations, while Figure 2h shows the same analysis, as the one illustrated in Figure 2g, but for different particle sizes. All coverage evolution conforms to the expected exponential trend. The authors note that higher concentrations do not necessarily ensure faster assembly and that an optimal concentration may exist. However, it is important to point out that concentration can be critical to achieve monolayer assembly in previous solution-based monolayer assembly methods, but our method is not sensitive to concentration. This can be a unique strength of our method where the monolayer assembly can tolerate errors in concentration control. Figures S10–S14 and their associated discussion can provide some clarification, but a detailed interdependence of the parameters α, C_0, and a_p requires further study. We hypothesize that higher concentrations eventually become detrimental to $g(u,v,w)$ (see the expression of α), thereby slowing down the assembly process. Nevertheless, the CSA method achieves monolayer assembly regardless of particle concentration and size within the testing range.

One potential application of producing large-scale self-assembled self-limiting films of micro/nanoparticles is structural coloration. In contrast to conventional coloration methods using organic molecules in pigments that are facing the challenge of instability and toxicity, colors from engineered architectures that are originally inspired by natural creatures offer promising alternative routes.[28−31] Particularly, dielectric structures enable high-quality optical resonance by reducing the material loss that is inevitable in metallic nanostructures.[32] Furthermore, creating 3D structures delivers more design freedom to cover a full range spectrum of colors.[33] However, the top-down lithography-based manufacturing is time-consuming, sophisticated, and cost-inefficient. Here, as a proof of concept, we used the obtained monolayer and stacked multiple monolayers of self-assembled SiO_2 particles to create different structure-induced colors recorded using our lab-made observing apparatus (Figure S15).

Figure 3a summarizes the colors observed in the monolayer films of self-assembled SiO_2 particles manufactured by CSA with different particle diameters: 487 nm diameter particles display a yellow color, 761 nm diameter particles display an orange color, and 1007 nm diameter particles display a blue color. The corresponding attenuation spectrum for 1007 nm diameter particles is shown in Figure 3b, where a clear resonance feature is observed. Figure 3b displays excellent agreement between finite-difference-time-domain (FDTD) simulation and experimental scattering spectra of our SiO_2 (1007 nm) monolayer particles. The scattering spectra of the other SiO_2 monolayer particles with different diameters can be found in Figure S17. Furthermore, the FDTD-simulated Ez-field profile in the $x-y$ plane shown in Figure 3c when the electromagnetic wave propagates along the z-axis suggests that the structural coloration derives from the magnetic dipole Mie resonance in the visible range. According to Mie theory,[34] the resonance peak depends on the refractive index of materials and scatterer dimensions. In Figure S16a,b, it is clear that the resonance peak shifts to red with an increasing diameter of nanospheres and refractive index of materials. During the CSA assembly process, the particles are accelerated by the acoustic wave and slammed onto the substrate. Considering the viscoelastic elasticity of

https://doi.org/10.1021/acsami.2c14149
ACS Appl. Mater. Interfaces XXXX, XXX, XXX−XXX

PDMS substrates, the particles would get partially embedded inside the substrate (Figure S18). As the refractive index of SiO_2 is close to PDMS, the embedment reduces the effective scattering volume of particles. Thus, we calculate the depth of SiO_2 particles (D_{dep}) inside the PDMS substrate (Figure S18). As demonstrated in Figure S16c, the simulated Mie scattering spectra as a function of D_{dep} indicate that larger D_{dep} causes blue shifting of the resonance peak.

Based on the parameters that can influence the transmission spectra mentioned above, we measured those parameters by AFM and SEM (Figure S17) and performed the calculations of converting measured and FDTD-simulated transmission spectra to colors. From Figure 3d, the calculation results display excellent agreement with experimental structural coloration under white light illumination. Furthermore, we calculate colors for a group of particles with different diameters and plot their color coordinates in the CIE1931 color space (see Figure 3e). The results show the color range of monolayer films of particles whose diameters range from 200 nm to 1500 nm. In addition, we stacked the monolayer samples (Figure 3f), and experimental colors of different combinations are summarized in Figure 3g. The results show that the stacked monolayers can significantly enrich the color map and the potential to create a full range of coloration.

In addition to functionality, it is important to consider the sustainability of manufacturing and usage. Nanoparticles and polymers can be hazardous when released into the ecosystem. Here, we have demonstrated the repairability and recyclability accommodated by the CSA method, as shown in Figure 4a. The digital images, SEM images, and corresponding structural colorations of the samples at different stages are compared in Figure 4b. To mimic the damage of coating during the application, we utilize a sticky PDMS stamp to detach the original SiO_2 particle monolayer from its original surface (Figure 4a). As compared in Figure 4b (top row), such damage can create nonuniformity in the coating leading to the loss of coloration. By performing the CSA process again in the SiO_2 particle solution, the blank regions are refilled with particles and the coloration is fully restored, as shown in Figure 4b (lower right). Because of the self-limiting mechanism, the reparation will terminate when a full monolayer is achieved. We have further examined the recyclability of the functional coating by washing the samples with IPA under sonication for 45 min (Figure 4a, left, and 4b, lower left). SiO_2 particles are completely removed leaving a clean transparent PDMS film, and SiO_2 particles can be collected in IPA solution for future applications.

CONCLUSIONS

In summary, CSA represents a high-quality and scalable self-limiting assembly method to achieve particle monolayers on flexible polymer substrates. Unlike chemisorption mechanisms for SAM, CSA highlights a new assembly mechanism in which physical collision and surface adhesion between particles and viscoelastic polymer substrates are modulated by acoustic and flow fields. The mechanism is independent of the chemical heterogeneity of polymer substrates and enables close-packed monolayers of particles on the polymer. CSA also unlocks a wide range of hard-to-wet systems that are desirable but extremely challenging to manufacture. The capability of accurately controlling the layer numbers of assemblies in the wafer scale and the capability to repair and recycle the coating and substrate materials pave the way toward next-generation flexible optics and wearable electronics.

EXPERIMENTAL SECTION

Modification of SiO_2 Particles. Three kinds of monodisperse silicon dioxide (SiO_2) spheres (Sigma-Aldrich; 500, 750, 1000 nm) are employed in this work. The diameters are further precisely determined by SEM images. The results show that the average diameters are 487 ± 10 nm, 761 ± 25 nm, and 1007 ± 29 nm, respectively. Because of the intrinsic hydrophilicity of SiO_2, we use (3-aminopropyl) triethoxysilane to modify it and transfer it into hydrophobicity. Briefly, 100 mg of SiO_2 particles are added to 10 mL of ethanol, followed by sonication for 5 min. Then, the solution is heated in an oil bath at 60 °C for 48 h. The resulting solution is finally centrifuged 5 times (each time for 5 min).

Self-Limiting Assembly of Monolayer. Polydimethylsiloxane film (PDMS) is fabricated on the surface of a glass slide (1 inch × 1 inch) using spin-coating method. The ratio of monomer and cross-linking agent is adjusted to 10:1 in volume. Note that this is for the assembly of SiO_2 particles, but 20:1 for the PMMA particle assembly. The PDMS fiber is prepared by stretching the uncured PDMS on a glass slide (heated to 100 °C). The patterned PDMS is made in a patterned Si wafer mold. Before assembly, the as-prepared hydrophobic particle solution is heated to 50 °C and kept in a sonicator. The spin-coated PDMS substrate then is held in the holder of a lab-made dip coater. During the dipping process, sonication is applied, and the sample is immersed in the solution all of the time.

Structural Coloration Simulation. To reveal the origin of the structural coloration produced by our CSA sample, we employed finite-difference time-domain method to fit experimental spectra of monolayer nanoparticles. To accelerate the simulation, we employ periodical boundary conditions because of the lattice structure in our samples, in which the refractive indices of SiO_2 and PDMS are set to be constant values, as $n_{SiO_2} = 1.45$ and $n_{PDMS} = 1.43$, respectively. A total field scattered field source is utilized to separate the scattered field from the total field, so that we can measure the scattering spectrum of particles that are illuminated by a plane wave.

The spectra are first converted to XYZ color coordinates using eqs 1−3

$$X = \int R(\lambda)\bar{x}(\lambda)\mathrm{d}\lambda \tag{1}$$

$$Y = \int R(\lambda)\bar{y}(\lambda)\mathrm{d}\lambda \tag{2}$$

$$Z = \int R(\lambda)\bar{z}(\lambda)\mathrm{d}\lambda \tag{3}$$

where $R(\lambda)$ is the scattering spectra; the color matching functions $\bar{x}(\lambda)$, $\bar{y}(\lambda)$, $\bar{z}(\lambda)$ defined by the International Commission on Illumination (CIE) are a numerical description of the response of the three types of cone cells in the human eye. After normalization using eq 2

$$x = \frac{X}{X+Y+Z}, y = \frac{Y}{X+Y+Z}, z = \frac{Z}{X+Y+Z} \tag{4}$$

only two parameters, x and y, are needed to locate the color position in the CIE1931 color space and convert the spectrum to color.

Characterization. Scanning electron microscope (SEM, Hitachi S-4800) is used to characterize the sample morphologies. The wettability is conducted using a lab-made contact angle measurement setup. The DI water droplet is ∼5 μL. The Fourier transform infrared (FT-IR, PerkinElmer) spectrum is conducted to characterize the surface chemistry of SiO_2 particles. The SiO_2 particle diameter and depth in PDMS are obtained by atomic force microscopy (AFM, Agilent 5500). The scattering spectra of monolayer SiO_2 particles are conducted by a Hitachi U4100 UV−vis−NIR spectrometer.

ASSOCIATED CONTENT

Supporting Information

The Supporting Information is available free of charge at https://pubs.acs.org/doi/10.1021/acsami.2c14149.

Roll-to-roll assembly process to enable wafer-scale manufacturing (MP4)

https://doi.org/10.1021/acsami.2c14149
ACS Appl. Mater. Interfaces XXXX, XXX, XXX−XXX

The setup of the acoustic + dipping process; SEM images, AFM images, and diameter distribution of monodisperse SiO_2 spheres; FT-IR spectra of pure and APTES-modified SiO_2 (APTES-SiO_2) spheres; contact angle measurement; pure SiO_2 particles (i.e., hydrophilic) assembled on PDMS substrate (10:1) using CSA; PMMA (~5 μm) particles assembled on PDMS substrate (20:1); the setup of roll-to-roll apparatus; SEM images of the assembly process of SiO_2 particles (761 nm to 10 mg mL^{-1}) using different assembly procedures; SEM images of the assembly process of SiO_2 nanoparticles (761 nm) with various concentrations; SEM images of the assembly process of SiO_2 nanoparticles (10 mg mL^{-1}) with different diameters; summary of values of $\alpha C_0 a_p$ for the assembly process using various SiO_2 nanoparticle diameters and concentrations; plane SEM images of assembled monolayer SiO_2 with various concentrations and diameters; cross-sectional SEM images of assembled monolayer SiO_2 with various concentrations and diameters; digital images of assembled monolayer particles on PDMS-coated glass slide; the setup of observation of structural coloration; scattering spectra simulation of monolayer SiO_2 nanoparticles using various parameters; experimental and simulation scattering spectra of monolayer SiO_2 particles; and the depth of SiO_2 particles into PDMS (10:1) substrate (PDF)

AUTHOR INFORMATION

Corresponding Author

Bo Li − *Department of Mechanical Engineering, Villanova University, Villanova, Pennsylvania 19085, United States; Hybrid Nano-Architectures and Advanced Manufacturing Laboratory, Villanova University, Villanova, Pennsylvania 19085, United States;* orcid.org/0000-0001-9766-7925; Email: bo.li@villanova.edu

Authors

Liang Zhao − *Department of Mechanical Engineering, Villanova University, Villanova, Pennsylvania 19085, United States; Hybrid Nano-Architectures and Advanced Manufacturing Laboratory, Villanova University, Villanova, Pennsylvania 19085, United States*

Bchara Sidnawi − *Department of Mechanical Engineering, Villanova University, Villanova, Pennsylvania 19085, United States; Cellular Biomechanics and Sports Science Laboratory, Villanova University, Villanova, Pennsylvania 19085, United States*

Jichao Fan − *Department of Electrical and Computer Engineering, The University of Utah, Salt Lake City, Utah 84112, United States*

Ruiyang Chen − *Department of Electrical and Computer Engineering, The University of Utah, Salt Lake City, Utah 84112, United States*

Thomas Scully − *Department of Mechanical Engineering, Villanova University, Villanova, Pennsylvania 19085, United States; Hybrid Nano-Architectures and Advanced Manufacturing Laboratory, Villanova University, Villanova, Pennsylvania 19085, United States*

Scott Dietrich − *Department of Physics, Villanova University, Villanova, Pennsylvania 19085, United States*

Weilu Gao − *Department of Electrical and Computer Engineering, The University of Utah, Salt Lake City, Utah 84112, United States;* orcid.org/0000-0003-3139-034X

Qianhong Wu − *Department of Mechanical Engineering, Villanova University, Villanova, Pennsylvania 19085, United States; Cellular Biomechanics and Sports Science Laboratory, Villanova University, Villanova, Pennsylvania 19085, United States;* orcid.org/0000-0002-6216-5674

Complete contact information is available at: https://pubs.acs.org/10.1021/acsami.2c14149

Author Contributions

B.S. and J.F. contributed equally to this work. B.L. conceived, initiated, and supervised the project. L.Z. conceived the experiment and performed the assembly, structural characterization including all SEM imaging, contact angle measurement and part of AFM measurement, and structural coloration characterization. B.S. performed the coverage of assembly and analysis and simulation of the assembly data. J.F. performed the analysis and simulation of structural coloration. R.C. performed the measurement of scattering spectra. T.S. constructed the roll-to-roll setup and performed part of the assembly. S.D. performed part of AFM measurement. W.G. designed and supervised the optical measurement and data analysis. Q.W. supervised physics-based modeling. All authors contributed to writing and revising the manuscript.

Notes

The authors declare the following competing financial interest(s): B. L., Q.W., Z.L., and B. S. have a U.S. Provisional Patent Application on the topic of this paper (63/405,98, 2022). The other authors declare no competing interests.

ACKNOWLEDGMENTS

L.Z., B.S., Q.W., and B.L. were partially supported by the National Science Foundation CMMI Advanced Manufacturing Program under Award # 2003077. L.Z. and B.L. acknowledge the startup fund of Villanova University. J.F., R.C., and W.G. acknowledge the startup fund of the University of Utah.

REFERENCES

(1) Akkerman, H. B.; Blom, P. W.; De Leeuw, D. M.; De Boer, B. Towards Molecular Electronics with Large-area Molecular Junctions. *Nature* **2006**, *441*, 69−72.

(2) Tao, N. J. Electron Transport in Molecular Junctions. *Nat. Nanotechnol.* **2006**, *1*, 173−181.

(3) Carnegie, C.; Urbieta, M.; Chikkaraddy, R.; de Nijs, B.; Griffiths, J.; Deacon, W. M.; Kamp, M.; Zabala, N.; Aizpurua, J.; Baumberg, J. J. Flickering Nanometre-scale Disorder in a Crystal Lattice Tracked by Plasmonic Flare Light Emission. *Nat. Commun.* **2020**, *11*, No. 682.

(4) Sekitani, T.; Zschieschang, U.; Klauk, H.; Someya, T. Flexible Organic Transistors and Circuits with Extreme Bending Stability. *Nat. Mater.* **2010**, *9*, 1015−1022.

(5) Klauk, H.; Zschieschang, U.; Pflaum, J.; Halik, M. Ultralow-power Organic Complementary Circuits. *Nature* **2007**, *445*, 745−748.

(6) Calhoun, M. F.; Sanchez, J.; Olaya, D.; Gershenson, M.; Podzorov, V. Electronic Functionalization of the Surface of Organic Semiconductors with Self-assembled Monolayers. *Nat. Mater.* **2008**, *7*, 84−89.

(7) Litke, J. L.; Jaffrey, S. R. Highly Efficient Expression of Circular RNA Aptamers in Cells Using Autocatalytic Transcripts. *Nat. Biotechnol.* **2019**, *37*, 667−675.

(8) Ren, S.; Yang, S.; Zhao, Y.; Zhou, J.; Xu, T.; Liu, W. Friction and Wear Studies of Octadecyltrichlorosilane SAM on Silicon. *Tribol. Lett.* **2002**, *13*, 233−239.

(9) Yu, J.; Kan, Y.; Rapp, M.; Danner, E.; Wei, W.; Das, S.; Miller, D. R.; Chen, Y.; Waite, J. H.; Israelachvili, J. N. Adaptive Hydrophobic and Hydrophilic Interactions of Mussel Foot Proteins with Organic Thin Films. *Proc. Natl. Acad. Sci. U.S.A.* **2013**, *110*, 15680−15685.

(10) Horinek, D.; Netz, R. R. Specific Ion Adsorption at Hydrophobic Solid Surfaces. *Phys. Rev. Lett.* **2007**, *99*, No. 226104.
(11) Ohya, Y.; Miyoshi, N.; Hashizume, M.; Tamaki, T.; Uehara, T.; Shingubara, S.; Kuzuya, A. Formation of 1D and 2D Gold Nanoparticle Arrays by Divalent DNA-gold Nanoparticle Conjugates. *Small* **2012**, *8*, 2335−2340.
(12) Xiang, J.; Zhu, P.; Masuda, Y.; Koumoto, K. Fabrication of Self-assembled Monolayers (SAMs) and Inorganic Micropattern on Flexible Polymer Substrate. *Langmuir* **2004**, *20*, 3278−3283.
(13) Bain, C. D.; Whitesides, G. M. Molecular-level Control over Surface Order in Self-assembled Monolayer Films of Thiols on Gold. *Science* **1988**, *240*, 62−63.
(14) Park, J. S.; Lee, Y.-J.; Yoon, K. B. Marked Increase in the Binding Strength between the Substrate and the Covalently Attached Monolayers of Zeolite Microcrystals by Lateral Molecular Cross-linking between the Neighboring Microcrystals. *J. Am. Chem. Soc.* **2004**, *126*, 1934−1935.
(15) Bigioni, T. P.; Lin, X.-M.; Nguyen, T. T.; Corwin, E. I.; Witten, T. A.; Jaeger, H. M. Kinetically Driven Self Assembly of Highly Ordered Nanoparticle Monolayers. *Nat. Mater.* **2006**, *5*, 265−270.
(16) Freeman, R. G.; Grabar, K. C.; Allison, K. J.; Bright, R. M.; Davis, J. A.; Guthrie, A. P.; Hommer, M. B.; Jackson, M. A.; Smith, P. C.; Walter, D. G.; Natan, M. J. Self-assembled Metal Colloid Monolayers: an Approach to SERS Substrates. *Science* **1995**, *267*, 1629−1632.
(17) Genzer, J.; Efimenko, K. Creating Long-lived Superhydrophobic Polymer Surfaces through Mechanically Assembled Monolayers. *Science* **2000**, *290*, 2130−2133.
(18) Gholamrezaie, F.; Mathijssen, S. G.; Smits, E. C.; Geuns, T. C.; van Hal, P. A.; Ponomarenko, S. A.; Flesch, H.-G.; Resel, R.; Cantatore, E.; Blom, P. W.; de Leeuw, D. M. Ordered Semiconducting Self-assembled Monolayers on Polymeric Surfaces Utilized in Organic Integrated Circuits. *Nano Lett.* **2010**, *10*, 1998−2002.
(19) Zhang, B.; Zhou, M.; Liu, X. Monolayer Assembly of Oriented Zeolite Crystals on α-Al_2O_3 Supported Polymer Thin Films. *Adv. Mater.* **2008**, *20*, 2183−2189.
(20) García Núñez, C.; Navaraj, W. T.; Liu, F.; Shakthivel, D.; Dahiya, R. Large-area self-assembly of Silica Microspheres/Nanospheres by Temperature-assisted Dip-coating. *ACS Appl. Mater. Interfaces* **2018**, *10*, 3058−3068.
(21) Ogi, T.; Modesto-Lopez, L. B.; Iskandar, F.; Okuyama, K. Fabrication of a Large Area Monolayer of Silica Particles on a Sapphire Substrate by a Spin Coating Method. *Colloid Surface A* **2007**, *297*, 71−78.
(22) Khanna, S.; Marathey, P.; Chaliyawala, H.; Rajaram, N.; Roy, D.; Banerjee, R.; Mukhopadhyay, I.; et al. Fabrication of Long-ranged Close-packed Monolayer of Silica Nanospheres by Spin Coating. *Colloid Surface A* **2018**, *553*, 520−527.
(23) Cagnani, G. R.; Spada, E. R.; Cagnani, L. D.; Torres, B. B.; Balogh, D. T.; Bardosova, M.; Faria, R. M. Large-area Flexible 2D-colloidal Crystals Produced Directly Using Roll-to-roll Processing. *Colloid Surface A* **2020**, *588*, No. 124389.
(24) Puebla-Hellmann, G.; Venkatesan, K.; Mayor, M.; Lörtscher, E. Metallic Nanoparticle Contacts for High-yield, Ambient-stable Molecular-monolayer Devices. *Nature* **2018**, *559*, 232−235.
(25) Zhou, D.; Hao, J.; Clark, A.; Kim, K.; Zhu, L.; Liu, J.; Cheng, X.; Li, B. Sono-assisted Surface Energy Driven Assembly of 2D Materials on Flexible Polymer Substrates: A Green Assembly Method Using Water. *ACS Appl. Mater. Interfaces* **2019**, *11*, 33458−33464.
(26) Zhou, D.; Han, M.; Sidnawi, B.; Wu, Q.; Gogotsi, Y.; Li, B. Ultrafast Assembly and Healing of Nanomaterial Networks on Polymer Substrates for Flexible Hybrid Electronics. *Appl. Mater. Today* **2021**, *22*, No. 100956.
(27) Sidnawi, B.; Zhou, D.; Li, B.; Wu, Q. A Physics-based Statistical Model for Nanoparticle Deposition. *J. Appl. Phys.* **2021**, *129*, No. 065303.
(28) Zhao, Y.; Xie, Z.; Gu, H.; Zhu, C.; Gu, Z. Bio-inspired Variable Structural Color Materials. *Chem. Soc. Rev.* **2012**, *41*, 3297−3317.
(29) Kinoshita, S.; Yoshioka, S. Structural Colors in Nature: the Role of Regularity and Irregularity in the Structure. *ChemPhysChem* **2005**, *6*, 1442−1459.
(30) Vukusic, P.; Sambles, J. R. Photonic Structures in Biology. *Nature* **2003**, *424*, 852−855.
(31) Kim, H.; Ge, J.; Kim, J.; Choi, S.-e.; Lee, H.; Lee, H.; Park, W.; Yin, Y.; Kwon, S. Structural Colour Printing Using a Magnetically Tunable and Lithographically Fixable Photonic Crystal. *Nat. Photonics* **2009**, *3*, 534−540.
(32) Song, M.; Wang, D.; Peana, S.; Choudhury, S.; Nyga, P.; Kudyshev, Z. A.; Yu, H.; Boltasseva, A.; Shalaev, V. M.; Kildishev, A. V. Colors with Plasmonic Nanostructures: A Full-spectrum Review. *Appl. Phys. Rev.* **2019**, *6*, No. 041308.
(33) Iwata, M.; Teshima, M.; Seki, T.; Yoshioka, S.; Takeoka, Y. Bio-inspired Bright Structurally Colored Colloidal Amorphous Array Enhanced by Controlling Thickness and Black Background. *Adv. Mater.* **2017**, *29*, No. 1605050.
(34) Hergert, W.; Wriedt, T.The Mie Theory: Basics and Applications; *Springer*, 2012; p. 169.

https://doi.org/10.1021/acsami.2c14149
ACS Appl. Mater. Interfaces XXXX, XXX, XXX−XXX